Chemical Engineering Journal 161 (2010) 204–211

Contents lists available at ScienceDirect

Chemical Engineering Journal

journal homepage: www.elsevier.com/locate/cej

Combined oxidation and reforming of methane to produce pure H_2 in a membrane reactor

J.F. Múnera, C. Carrara, L.M. Cornaglia, E.A. Lombardo*

Instituto de Investigaciones en Catálisis y Petroquímica - INCAPE (FIQ, UNL-CONICET), Santiago del Estero 2829, Santa Fe 3000, Argentina

ARTICLE INFO

Article history:
Received 21 December 2009
Received in revised form 7 April 2010
Accepted 13 April 2010

Keywords:
Combined reforming
Hydrogen selective membrane
Supported Rh catalysts

ABSTRACT

The combination of CO_2 reforming and oxidation of methane is currently being studied in conventional reactors trying to improve the energy balance in the production of synthesis gas. In this work, we applied the same concept to membrane reactors used to produce pure H_2. Two catalysts were used, Rh(0.6)/La_2O_3 and Rh(0.6)/La_2O_3(27)–SiO_2. They were first assayed in a conventional fixed-bed reactor (CR) in order to test their activity and stability before being used in the membrane reactor (MR). The latter was especially designed to detect the presence of hot spots in the catalyst bed and avoid the contact of O_2 rich atmospheres at high temperature (823 K) with the Pd–Ag membrane. Varying O_2 contents (0–10%) and CO_2/CH_4 ratios between 0.5 and 1.9 were fed to the membrane reactor to quantify their effect upon methane conversion and H_2 production and recovery through the membrane. The fresh, reduced and used catalysts were characterized through XRD, laser Raman spectroscopy and XPS. The spectroscopic features were consistent with the catalytic behavior of both formulations. The best performance of the MR was achieved using Rh supported on the binary oxide, 10% O_2 and CO_2/CH_4 = 1.9.

1. Introduction

Rhodium-based catalytic systems supported on La_2O_3 and La_2O_3–SiO_2 are active and stable for the dry reforming of methane (DRM) [1,2]. In order to produce ultrapure H_2, this reaction can be carried out in a membrane reactor with the additional benefit of overcoming the thermodynamic limitations of the endothermic reaction, thus allowing the attainment of higher methane conversions at lower temperatures. For this reaction, we and others have reported that the CH_4 conversion can be greatly improved by removing the hydrogen formed with a stable and highly selective dense Pd–Ag membrane [3–5]. Ferreira-Aparicio et al. used a Ni-catalyst in a membrane reactor and showed similar results [6]. However, one problem lies in the high-energy requirement of this reaction. In order to decrease the energy consumption, its coupling with the exothermic oxidation of methane has been considered. This explains the increased number of publications appeared in recent years concerning the combination of CO_2 reforming and partial oxidation of methane leading to more efficient routes for the conversion of natural gas to syngas [7,8]. This process has low-energy requirements due to the opposite contribution of the exothermic methane oxidation and the endothermic CO_2 reforming.

Since the rate of reaction of $CH_4 + O_2$ is no less than two orders of magnitude faster than the reforming of methane, the development of hot spots at the catalyst bed entrance is almost unavoidable. These hot spots may reach ca. one hundred degrees in a conventional fixed-bed reactor as shown by Simeone et al. [9]. This is particularly critical in the case of membrane reactors because the contact at high temperature of O_2 containing feed streams with the Pd–Ag membrane is almost certain to lead to the formation of pinholes with the consequent drop in H_2 selectivity and the eventual collapse of the alloy layer [10]. This requires an adequate design of the catalyst bed to avoid the rapid deterioration of the membrane.

In this work, we report the results obtained in both a conventional and a Pd–Ag membrane reactor using Rh supported on either La_2O_3 or La_2O_3(27)–SiO_2 to catalyze the partial oxidation and reforming of methane (combined reforming of methane – CRM). The catalytic stability of both formulations was also studied. The catalysts were characterized before and after use with a battery of instrumental techniques in order to understand the relationship between their catalytic behavior and physicochemical features.

2. Experimental

2.1. Catalyst synthesis

The Rh(0.6)/La_2O_3 catalyst was prepared by conventional wet impregnation of La_2O_3 (Alfa Aesar 99.99%) using $RhCl_3 \cdot 3H_2O$.

* Corresponding author. Tel.: +543424536861; fax: +543424536861.
E-mail address: nfisico@fiq.unl.edu.ar (E.A. Lombardo).

1385-8947/$ – see front matter © 2010 Elsevier B.V. All rights reserved.
doi:10.1016/j.cej.2010.04.022

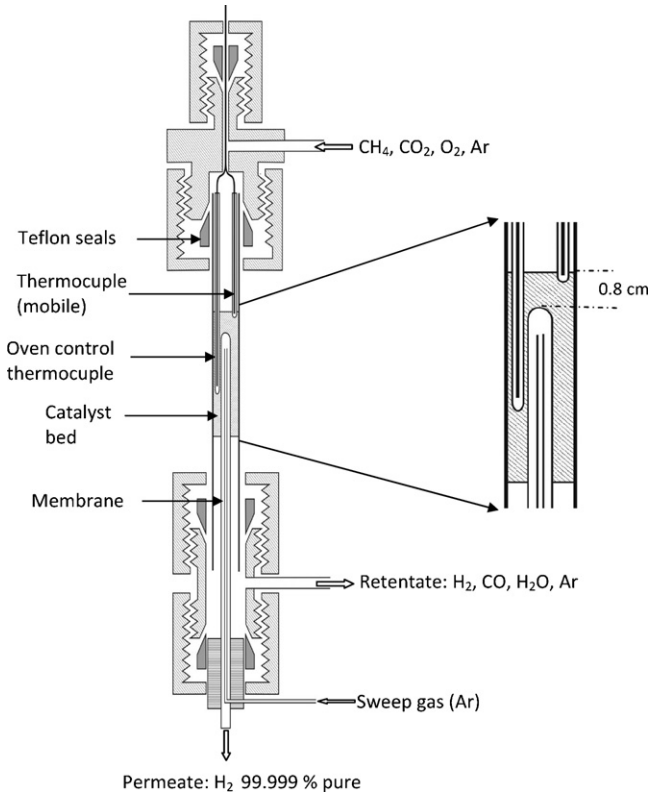

Fig. 1. Membrane reactor (MR) built using a commercial (REB Research) self-supporting Pd–Ag membrane.

The $La_2O_3(27)$–SiO_2 support was prepared by incipient wetness impregnation of silica with lanthanum nitrate and calcined at 873 K for 5 h. The La_2O_3 load in the binary support was 27 wt.%. $Rh(0.6)/La_2O_3(27)$–SiO_2 was prepared by incipient wetness impregnation with $RhCl_3{\cdot}3H_2O$ followed by calcination at 823 K in air for 6 h. The metal load in both formulations was 0.6 wt.%.

2.2. Catalytic tests

2.2.1. Stability tests in a conventional reactor (CR)

Although these catalysts were shown to be stable for at least 100 h under DRM conditions [1,2], they were never tested in the presence of O_2 under reaction conditions. This is why in the stability tests, they were contacted with different feed streams to evaluate their performance for DRM, combined reforming (CRM), partial oxidation of methane (POM) and back to DRM in a conventional reactor of o.d. 0.5 cm. A thermocouple in a quartz sleeve was placed on top of the catalyst bed (50 mg).

2.2.2. Membrane reactor (MR)

The double tubular membrane reactor (i.d. 1.6 cm) (Fig. 1) was built using a commercial dense Pd–Ag alloy (o.d. 0.31 cm) (REB Research and Consulting), with one end closed and provided with an inner tube (o.d. 0.158 cm) to allow sweep gas (SG) flow. Two thermocouples were used: one inserted in the bed, which was connected to the oven temperature controller, and the other located at the top of the bed to check the presence of hot spots. The catalyst ($dp \leq 0.15$ mm) was diluted with quartz chips (70 mesh) to achieve a height of either 4.6 cm or 5.8 cm. In both cases, the bed started 0.8 cm above the top of the membrane (see details in Fig. 1). As said above, the reaction rate of methane with O_2 is about two orders of magnitude faster than with either CO_2 or H_2O [8,11]. Therefore, this bed design allowed the oxidation reaction to occur in the top region of the catalyst bed, well above the beginning of the membrane (*vide infra*). Before reaction, the catalyst was heated up to 823 K in Ar stream and reduced in situ in H_2 flow at 823 K for 2 h. Different CH_4:CO_2:O_2:Ar ratios were employed with O_2 concentrations between 3 and 10%. The reaction temperature was 823 K in all cases. To study the CO_2/CH_4 ratio effect upon hydrogen production, the following [CH_4:CO_2:O_2:Ar] ratios were employed: [1:0.5:0.3:1.4], [1:1:0.3:0.9] and [1:1.9:0.3:0.0]. In all these cases the ratio CH_4:O_2 = 3.3.

The feed gases and the reaction products were analyzed with two on-line thermal conductivity detector gas chromatographs: a Shimadzu GC-8A and a SRI. The former instrument was equipped with a Porapak column, and the latter with a molecular sieve column.

2.3. Catalyst characterization

2.3.1. X-ray diffraction (XRD)

The XRD patterns of the calcined and used solids were obtained with an XD-D1 Shimadzu instrument, using Cu Kα radiation at 30 kV and 40 mA. The scanning rate was 1.0°/min for 2θ values between 10° and 70°.

2.3.2. Laser Raman spectroscopy

The Raman spectra were recorded using a LabRam spectrometer (Horiba-Jobin-Yvon) coupled to an Olympus confocal microscope (a 100× objective lens was used for simultaneous illumination and collection), equipped with a CCD detector cooled to about 200 K using Peltier effect. The excitation wavelength was in all cases 532 nm (Spectra Physics argon-ion laser). The laser power was set at 30 mW. Integration times ranged from a few seconds to a few minutes, depending on the sample.

2.3.3. X-ray photoelectron spectroscopy

The XPS measurements were carried out using a multitechnique system (SPECS) equipped with a dual Mg/Al X-ray source and a hemispherical PHOIBOS 150 analyzer operating in the fixed analyzer transmission (FAT) mode. The spectra were obtained with pass energy of 30 eV; the Mg Kα X-ray source was operated at 200 W and 12 kV. The working pressure in the analyzing chamber was less than 6×10^{-7} Pa.

The data were processed with the Casa XPS program (Casa Software Ltd., UK). The peak areas were determined by integration employing a Shirley-type background. Peaks were considered to be a mix of Gaussian and Lorentzian functions in a 70/30 ratio. For the quantification of the elements, sensitivity factors provided by the manufacturer were used.

3. Results and discussion

3.1. Activity and stability in different reaction atmospheres

Before using the catalysts in the membrane reactor, it was necessary to verify the stability of both formulations in a conventional reactor. The catalytic activity and stability of the $Rh(0.6)/La_2O_3$ and $Rh(0.6)/La_2O_3(27)$–SiO_2 solids are shown in Fig. 2. The catalysts went through 30 h long cycles of DRM, partial oxidation of methane (POM), CRM and back to DRM. The experiments were carried out at 823 K, 50 K below the maximum temperature allowed for the Pd–Ag membrane when it is exposed to a reducing atmosphere. For the DRM reaction, the CO_2 conversion was higher than the CH_4 conversion due to the occurrence of the reverse water gas shift reaction (RWGS) in which CO_2 reacted with the H_2 produced in the reforming reaction. It was observed that the methane conversion increased and the carbon dioxide conversion decreased (not shown) when oxygen was added to the feed stream (CRM), symptomatic of the occurrence of the total oxidation of methane. As a

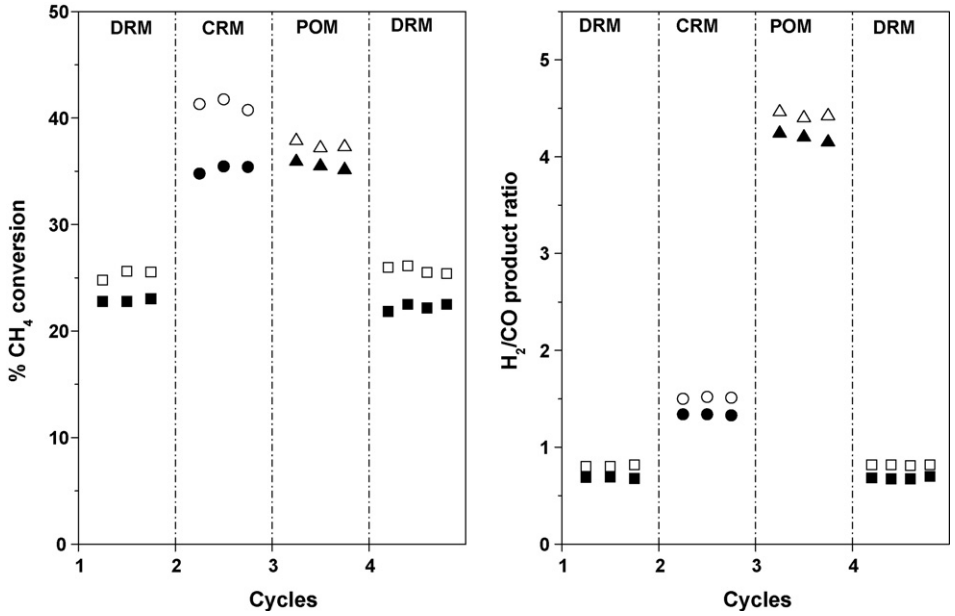

Fig. 2. Catalytic behavior and stability in a conventional fixed-bed flow reactor (CR). Rh/La_2O_3 (full symbols) and Rh/La_2O_3–SiO_2 (empty symbols). $T = 823$ K, $W/F = 1.7 \times 10^{-5}$ g h ml^{-1}, CH_4:CO_2:O_2:Ar feed ratios: DRM [1:1:0:1.2], POM [1:0:0.2:1.6] and CRM [1:1:0.33:0.67], cycle length: 30 h.

consequence of the occurrence of both reactions, a higher H_2/CO ratio was obtained, in agreement with what has been reported by other authors [12,13]. In the case of POM, the H_2/CO ratio was close to 4 and the H_2O/CO_2 ratio (not shown) was equal to 0.45. Note that for the total oxidation of methane, the stoichiometric H_2O/CO_2 ratio is 2, indicating that the WGS reaction ($CO + H_2O \Leftrightarrow CO_2 + H_2$) produced more CO_2 and consequently increased the H_2/CO ratio. Both catalytic systems were stable for at least 120 h on stream, total duration of the four-cycle tests (Fig. 2).

3.2. Oxygen consumption during CRM

To evaluate the contribution of the upper part of the bed (membrane reactor) to the overall reaction, a specially designed experiment was carried out. A quartz tube of the same diameter as the shell of the MR was loaded with the amount of catalyst needed for a bed height of 0.8 cm. The reaction mixture contained CH_4, CO_2, O_2 and Ar. Substituting Ar by CO_2, it was possible to modify the CO_2/CH_4 ratio between 0.5 and 1.9 without changing the partial pressures of CH_4 and O_2. In all cases, the total consumption of O_2 was observed (Fig. 3a) and a temperature difference close to 10 K was detected using two thermocouples, one located at the top and the other at the center of the bed. As expected, Fig. 3a shows that in the presence of O_2, the CO_2 conversion decreases due to the contribution of a total combustion of methane to the CO_2 balance. The change in methane conversion is consistent with the CO_2 evolution. Fig. 3b shows the product composition when the feed stream contained 10% O_2. A steady increase is observed in the concentration of both H_2O and CO, while H_2 shows a maximum at $CO_2/CH_4 = 1.0$. The decay above this ratio may be due to the enhanced simultaneous occurrence of the RWGS which would be favored by excess CO_2.

The data shown in Fig. 3 and Table 1 indicate that in the first part of the reactor, in addition to methane oxidation, two endothermic reactions (RWGS and DRM) occur. Note that the equilibration ratios ($\eta = \prod_i p_i^{\upsilon i}/K_{eq}$) for both DRM and RWGS were always close to 1. These findings suggest that at the beginning of the membrane (0.8 cm below the top of the catalyst bed) the system is in thermodynamic equilibrium considering both the DRM and RWGS reactions. From the above, it is concluded that the role of the catalytic bed in contact with the membrane would be to restore the thermodynamic equilibrium as hydrogen is being removed through the inner tube wall.

3.3. Effect of oxygen addition upon the dry reforming of methane in a membrane reactor

The dry reforming reaction is highly endothermic. Adding oxygen to the reformer will reduce the need for external heating. In order to improve both the system energy balance and the hydrogen production, and at the same time, smooth out the hot spots that may develop in the catalyst bed, the effect of oxygen concentration added to the feed stream (3–10%) was explored. Fig. 4 shows the methane conversion and hydrogen permeation across the palladium–silver membrane for several oxygen concentrations (3–10%) and different fluxes of sweep gas using $Rh(0.6)/La_2O_3$ as catalyst. Increasing the O_2 content enhanced the CH_4 conversion and at the same time drastically reduced the CO_2 conversion (not shown). The best results were obtained with 10% O_2, which corresponds to a CH_4/O_2 ratio of 3.3. Similarly to what happened in the CR, a temperature difference between 5 and 10 K was measured in the MR when feeding 10% O_2. When the system was operated even with 10 ml/min of SG flow rate, the CH_4 conversion significantly increased (45%) in comparison with the system operated under dry reforming conditions. This is due to the methane consumption in both the oxidation and reforming reactions. However, the CH_4 conversion showed a low enhancement compared to the thermodynamic equilibrium values (Table 1).

The chemical equilibrium analysis of combined CH_4-reforming with CO_2 and O_2 conducted by total Gibbs energy minimization using Lagrange's undetermined multiplier method was reported by Aishah et al. [7]. They determined that the optimum CH_4/O_2 ratio was ca. 3 for the combined reaction conducted in a conventional reactor with $CH_4/CO_2 = 1$, feed ratio. Our results agree with their findings.

Note that the MR experiments were performed in the reactor shown in Fig. 1. In this system, the O_2 was totally consumed before reaching the top of the membrane (Section 3.2). Therefore, no contact of the membrane with oxygen rich mixtures occurred, thus increasing the life of the Pd–Ag membrane that so far has lasted for 1800 h on stream.

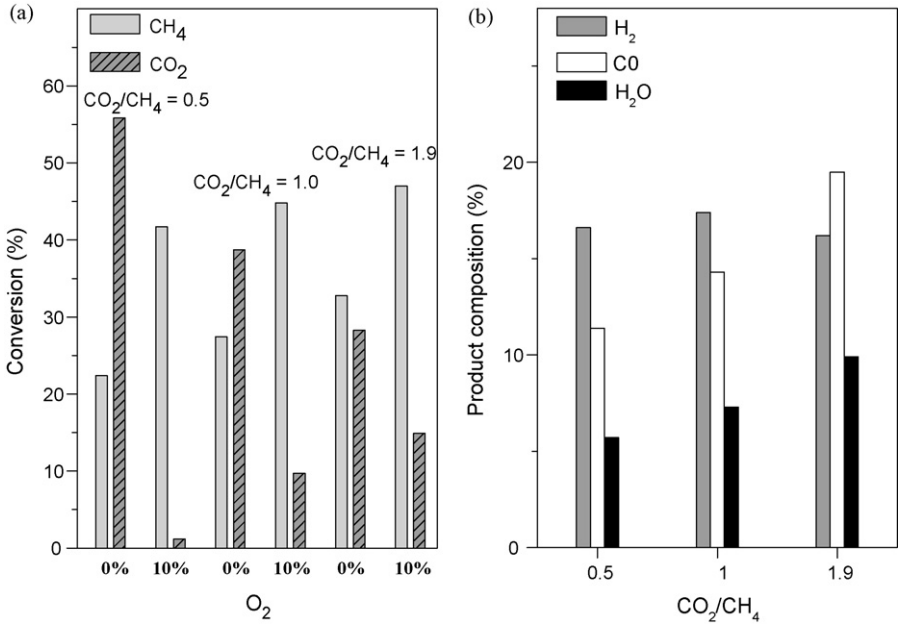

Fig. 3. Contribution of the upper part of the bed (MR) to the overall reaction. CR with the same i.d. as the MR, bed height 0.8 cm. To vary the CO_2/CH_4 ratio the following CH_4:CO_2:O_2:Ar ratios were employed: [1:0.5:0.3:1.4], [1:1:0.3:0.9] and [1:1.9:0.3:0.0]. In all cases the ratio CH_4:O_2 = 3.3, M = 0.15 g, $W/F = 1.5 \times 10^{-4}$ g h ml^{-1}, P = 1 atm, T = 823 K. In no case was oxygen detected at the reactor exit. (a) Conversions with and without O_2 fed and (b) product composition with 10% O_2 fed.

3.4. Comparison of catalysts

Fig. 5 compares the behavior of the Rh catalysts in the dry and combined reforming reactions. Note that the catalyst bed is 4.6 cm long albeit only 3.8 cm are in contact with the membrane. This corresponds to a permeation area equal to 3.8×10^{-4} m^2. Both catalysts yield an increase in methane conversion consistent with an enhancement of permeated H_2. The Rh(0.6)/La_2O_3(27)–SiO_2 catalyst exhibits the best behavior for DRM and CRM as shown by the increased methane conversion and hydrogen production.

Another parameter that matters in the comparison of catalysts is their ability to restore the equilibrium when H_2 is extracted from the shell side of the reactor. This behavior is quantified through the equilibration ratio (η) that should stay close to unity even at the highest sweep gas flow rate. Fig. 6 shows the behavior of both catalysts and clearly demonstrates that the binary oxide supported Rh is more effective than the Rh(0.6)/La_2O_3 formulation. When the SG flow rate increases, the difference between the methane conversion of both catalysts also increases. These results are in agreement with the ability to restore the equilibrium shown in Fig. 6. A similar behavior has been previously reported [3,14] for the dry reforming of methane. The metal dispersion is a critically important parameter in catalytic behavior. The high dispersion of the metal on the binary oxide support would be responsible for the higher reaction rates of these solids [3].

3.5. Effect of the CO_2/CH_4 feed ratio on the combined reforming reaction

Having shown the superior performance of the Rh/La–Si formulation, only this catalyst was used to explore the effect of the CO_2/CH_4 ratio upon the catalytic performance (Fig. 7). In Fig. 7a, the textured filling corresponds to the contribution of the membrane to the global process for several CO_2/CH_4 ratios, while the smooth filling shows the conventional reactor conversions obtained employing the configuration described in Section 3.2. Note that the effect of CO_2 upon methane conversion is very much limited in the conventional reactor but is amplified in the membrane reactor, in agreement with the increased hydrogen permeation shown in Fig. 7b. This confirms that proper control of

Table 1
Product composition at the outlet of the CR with a bed height of 0.8 cm[a].

CO_2/CH_4[b]	$\%O_2$[b]	XCH_4[c]	XCH_4[d]	XCO_2[c]	XCO_2[d]	$\%CH_4$[e]	$\%CO_2$[e]	%CO[e]	$\%H_2$[e]	$\%H_20$[e]	ηDRM[f]	ηRWGS[f]
0.5	0	22.4	23.8	55.8	55.9	21.8	5.3	13.2	10.7	1.3	0.95	1.08
	10	41.7	43.7	1.2	0.3	15.9	12.7	11.4	16.6	5.7	0.99	1.08
1.0	0	27.4[g]	30.3	38.7[g]	41.4	19.5	14.2	18.1	12.1	2.9	0.99	1.07
	10	44.8[g]	47.2	9.7[g]	10.7	15.7	21.2	14.3	17.4	7.3	1.00	0.99
1.9	0	32.8	37.7	28.3	30.6	17.4	32.2	23.8	13.3	5.2	0.98	1.02
	10	47.0	51.9	14.9	13.6	14.1	39.9	19.5	16.2	9.9	0.99	1.06

[a] Reactor i.d.:1.6 cm equal to the i.d. of the MR. $W/F = 1.5 \times 10^{-4}$ ml h g^{-1}, flow rate = 970 ml h^{-1}, temperature = 823 K, P = 1 atm.
[b] Feed compositions, balance Ar.
[c] CH_4 and CO_2 conversions.
[d] Equilibrium conversion values calculated with the program STANJAN.
[e] Outlet compositions.
[f] Equilibration ratios.
[g] These values did not change when W/F was doubled.

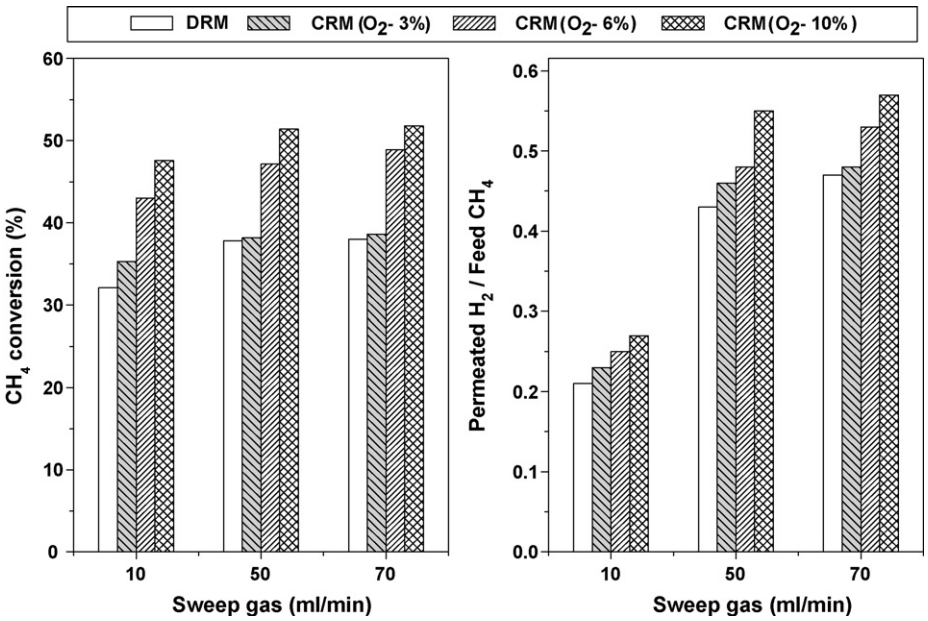

Fig. 4. Effect of oxygen added upon conversion and permeated H_2 (MR). Catalyst: Rh(0.6)/La_2O_3, membrane area = 3.8 cm^2, M = 1.5 g, $W/F = 1.5 \times 10^{-3}$ g h ml^{-1}, P = 1 atm, T = 823 K.

the CH_4:CO_2:O_2 ratio is essential to improve H_2 production. It should be noted that no experimental work concerning the combined reaction using membrane reactors has yet been published. Coming back to conventional reactors, Donazzi et al. [8] using Rh/Al_2O_3 studied the effect of the CO_2/CH_4 ratio between 1 and 3 upon CH_4 conversion. They reported that the greatest increase occurred between 1 and 2. This is in good agreement with our results in the MR, with a CO_2/CH_4 = 1.9 at the highest SG flow rate, where we observed an increase of methane conversion close to 40% (Figs. 3 and 7).

The CO_2 excess in the reactant mixture with respect to the dry reforming reaction stoichiometry favors the occurrence of the reverse water gas shift (RWGS) reaction. This secondary process consuming CO_2 and the produced H_2 leads to a large increase in the CO/H_2 ratio at the outlet of a conventional reactor (Fig. 3b). However, in the case of a membrane reactor the situation is different because H_2 is being extracted from the reaction side (retentate). Ferreira-Aparicio et al. [6] employed a highly selective Pd film (12–35 μm) supported on porous stainless steel and several Ni-based catalysts in a membrane reactor for the dry reforming reaction. They found that a CO_2 excess in the feed stream with respect to the stoichiometric ratio establishes more favorable conditions for the membrane reactor operation with lower carbon deposition. This is consistent with our results, which indicate that

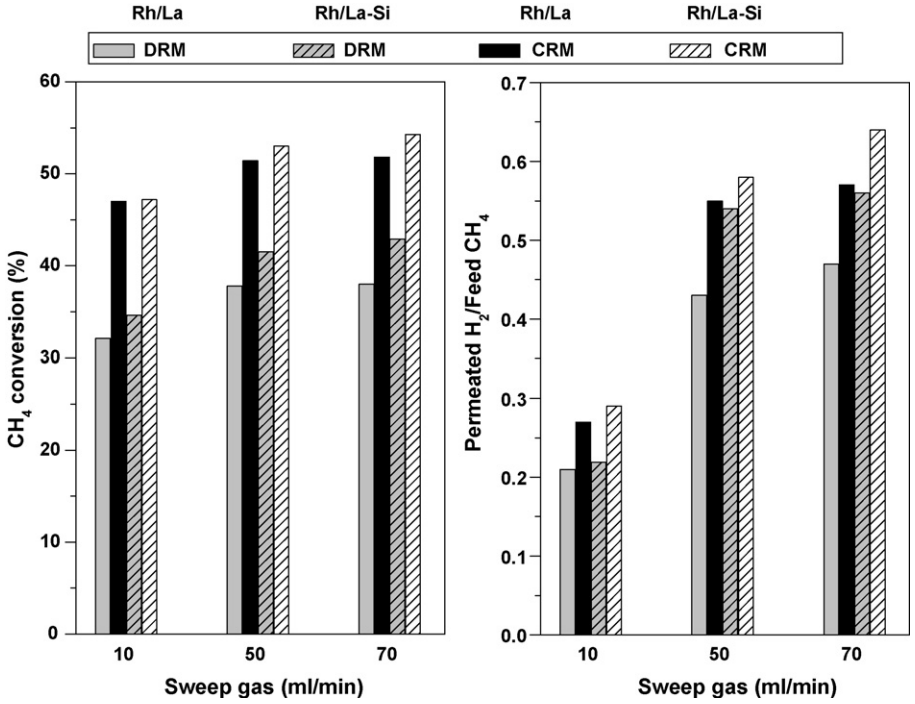

Fig. 5. Catalyst comparison (MR). Feed: CH_4:CO_2:O_2:Ar = 1:1:0.3:0.9. M = 1.5 g; $W/F = 1.5 \times 10^{-3}$ g h ml^{-1}, P = 1 atm, T = 823 K. Membrane area = 3.8 cm^2.

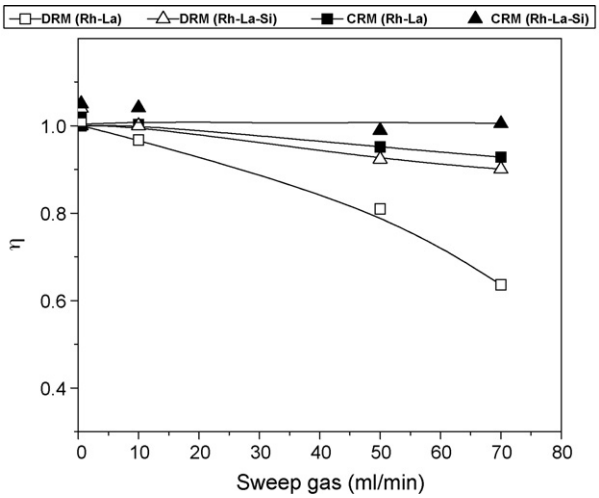

Fig. 6. Ability of the catalysts to keep the retentate equilibrated (MR). Catalysts: $Rh(0.6)/La_2O_3$ and $Rh(0.6)/La_2O_3(27)–SiO_2$, $M = 1.5$ g; $W/F = 1.5 \times 10^{-3}$ g h ml^{-1}, $P = 1$ atm, $T = 823$ K. Membrane area = 3.8 cm^2.

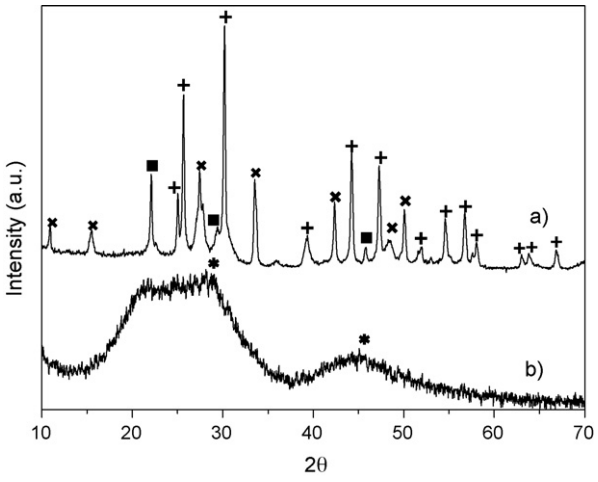

Fig. 8. XRD of the fresh solids. (a) $Rh(0.6)/La_2O_3$ and (b) Rh $(0.6)/La_2O_3(27)–SiO_2$. (*) $La_2Si_2O_7$, (■) $La_2O_2CO_3$, (+) $La(OH)_3$, (×) La_2O_3.

CO_2 excess increased H_2 production in the membrane reactor. Nevertheless, the CO_2 surplus in the feeding should not go beyond a certain level in order to reduce H_2 consumption.

3.6. Characterization of the used catalysts

3.6.1. X-ray diffraction (XRD)

The XRD pattern of $Rh(0.6)/La_2O_3(27)/SiO_2$ shows broad peaks centered around $2\theta = 28.8$ and 45.8 (Fig. 8) which correspond to the lanthanum disilicate phase $La_2Si_2O_7$ as previously reported by Vidal et al. [15]. In this pattern, an overlapping signal at $2\theta = 21^\circ$ is also observed which corresponds to the mostly amorphous SiO_2. Note that the X-ray diffractogram of the $Rh(0.6)/La_2O_3$ formulation shows the fingerprints of La_2O_3, $La(OH)_3$ and II-$La_2O_2CO_3$.

3.6.2. Laser Raman spectroscopy (LRS)

Raman spectroscopy is an effective tool to study properties of the different carbon materials [16], including catalytic carbon, carbon nanotubes, carbonaceous particles, carbon films and synthetic diamond. The first order transitions lie between 1200 and 1700 cm^{-1} [4].

Fig. 9 shows the characteristic bands of graphitic carbon deposits on both Rh catalysts recorded after the combined reaction was performed with different CO_2/CH_4 ratios. The three spectra have similar bands at 1350 (D mode) and 1590 cm^{-1} (G mode). The graphitic nature of carbon deposits can be deduced from the observation of the G and D bands. The band at 1590 named the G peak is the E2g mode of bulk graphite; its intensity scales with the crystal size. The band at 1350 was assigned to the analogue of the E2g mode for the graphite layers

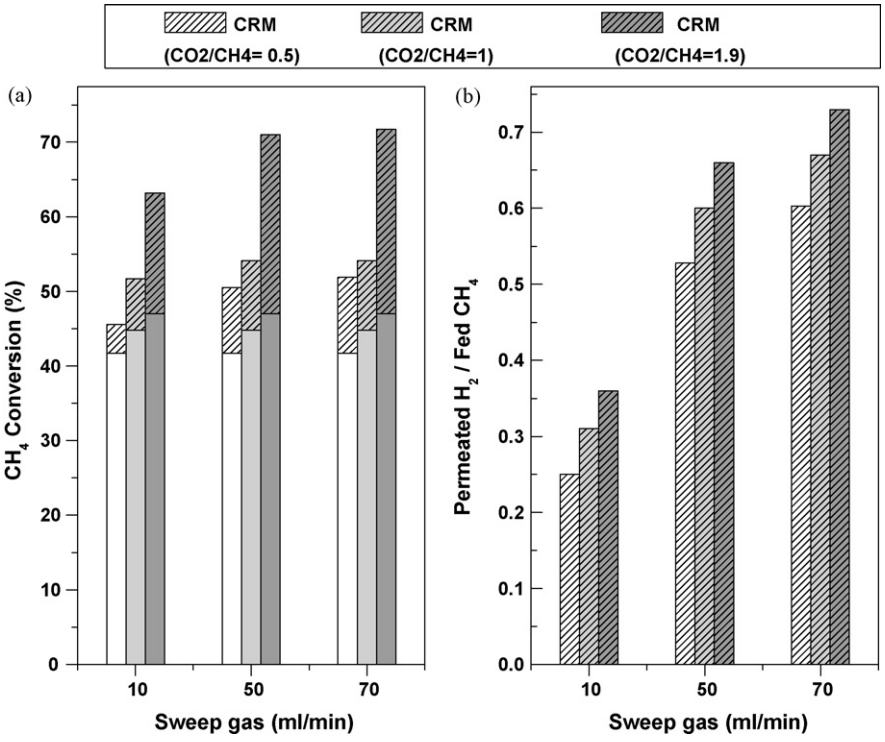

Fig. 7. Effect of the CO_2/CH_4 ratio upon methane conversion and H_2 permeation (MR). Catalyst: $Rh(0.6)/La_2O_3(27)–SiO_2$, $M = 1.5$ g, $W/F = 1.5 \times 10^{-3}$ g h ml^{-1}, $P = 1$ atm, $T = 823$ K. Membrane area = 5.0 cm^2.

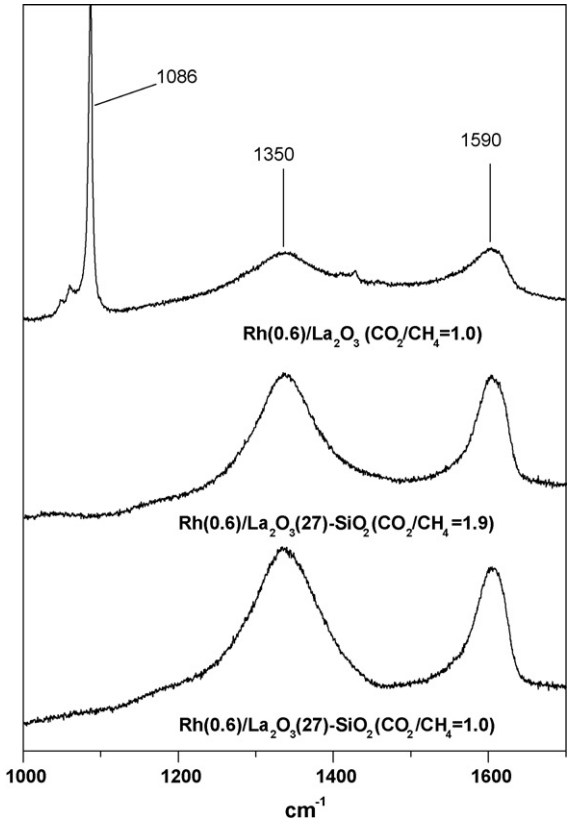

Fig. 9. Raman spectra of catalysts used in the CRM.

located at the boundary of the crystals and was designated E′2g or D.

Despite the fact that the used catalysts presented the characteristic bands of graphitic carbon, no carbon was detected through TGA measurements (detection limit of our instrument 0.1 μg/mg of catalyst). In agreement with the presence of only traces of carbon is the fact that no deactivation of the catalyst was observed after 120 h on stream. In the same vein, Connor and Ross [17] using a Pt/ZrO_2 catalyst found deactivation in the first hours in the dry reforming reaction due to carbon deposition; however, this was prevented with the addition of 11% oxygen to the CH_4/CO_2 mixture.

In the case of the $Rh(0.6)/La_2O_3$ catalyst another band at 1086 cm^{-1} was observed (Fig. 9) which belongs to lanthanum oxycarbonate. The presence of the carbonate group was also confirmed by the small bands recorded at the 1400–1450 cm^{-1} region. This species participates in the reaction mechanism, contributing to the oxidation of carbon deposited on the catalyst surface [1].

3.6.3. X-ray photoelectron spectroscopy

The intensity ratios and binding energies (BE) for the $Rh(0.6)/La_2O_3$ solid after calcination, in situ reduction at 723 K and after use in the methane reactions in a membrane reactor are given in Table 2. Binding energies were referenced to C 1s = 284.6 eV, which resulted in a binding energy for La $3d_{5/2}$ = 834.5 eV. For the calcined solid, the BE of Rh $3d_{5/2}$ was 308.1 eV. The broad peak (FWHM = 3.1 eV) suggests the presence of Rh^{3+} and Rh^{+} surface species. According to the literature, a high-energy value indicates the presence of Rh^{n+} species. Values in the 307.6–309.6 eV range for Rh^{+} compounds were compiled by Nefedov et al. [18]. However, other authors [19] reported BEs for Rh^{2+} compounds within a similar range (308.4–309.3 eV). The Rh^{3+} oxidation state presents a binding energy close to 309.7 eV [20]. In the case of pure Rh metal foil, the Rh $3d_{5/2}$ peak occurs at 307.0 eV, with 1.6 eV FWHM.

The Rh $3d_{5/2}$ peak is shifted to lower binding energies upon reduction, indicating the formation of Rh°. On the other hand, the DRM and CRM used catalysts show a Rh $3d_{5/2}$ BE slightly higher than the reduced sample and exhibit a larger FWHM. For the reduced and used catalysts, the Rh/La atomic ratios decreased compared to the calcined sample, suggesting that the rhodium dispersion was modified.

The C 1s spectra show two well-defined peaks at 284.4 and 289.2 eV. The peak at 289.1 ± 0.2 eV is attributed to carbonate carbon [21], consistent with the presence of the O 1s peak at 530.1 eV assigned to the lanthanum oxycarbonate species. The Raman spectrum (Fig. 9) also shows the characteristic band of oxycarbonates. In the case of the reduced solid, the intensity of the carbonate signal decreases (Table 2); however, the O/La ratio slightly increases and in the O 1s spectrum (not shown), a contribution at 528.0 eV appears, which is assigned to lattice oxygen [22]. After reaction, the O/La ratio shows a significant increase while the C_{CO_3}/La ratio decreases when the catalyst is used for CRM. The $C_{CO_3=}/O$ ratio is lower than the carbonate stoichiometric value ($C_{CO_3}/O = 0.33$) indicating that OH species are present on the surface. This last feature suggests that under the combined reforming reaction conditions, the catalyst surface contains a higher amount of surface hydroxyls. They are likely to come from a partial hydroxylation of the support surface in the presence of a higher concentration of water present in the reaction side when the CRM reaction is carried out.

The XPS intensity ratios and binding energies for the calcined, reduced and used $Rh(0.6)/La_2O_3(27)–SiO_2$ catalyst are given in Table 3. The catalyst was used in the membrane and in the conventional reactors, for the DRM and CRM reactions at 823 K with different CO_2/CH_4 ratios. For the calcined solid, the Rh 3d peak presents a FWHM = 4.8 eV, suggesting a mixture of Rh oxidation states. The result of the curve fitting considering two species is shown in Table 3; one appears at 308.8 eV and the other at 306.4 eV.

The reduced catalyst shows a line width and a binding energy lower than those of the calcined sample, indicating reduction to Rh°. The FWHM of the Rh $3d_{5/2}$ peak mainly reflects the particle size [21,23,24]. The reduced (fresh) and the used Rh catalysts show similar FWHM (3.1 eV). This indicates a similar average particle size in these samples and no surface oxidation was produced during the reaction. In agreement, the surface Rh/La ratio remained practically

Table 2
Binding energies[a] and surface atomic ratios for $Rh(0.6)/La_2O_3$.

Treatment	C 1s $C_{CO_3=}$ (eV)	Rh $3d_{5/2}$[c] (eV)	Rh/La	O/La	$C_{CO_3=}/La$	$C_{CO_3=}/O$
Calcined[b]	289.2	308.1 (3.1)	0.46	1.6	1.6	1.00
H_2 in situ[d] at 723 K	289.3	307.0 (1.8)	0.30	2.0	0.65	0.33
Used in MR[b] (DRM)CO_2/CH_4 = 1	289.3	307.2 (2.4)	0.25	6.9	1.6	0.23
Used in MR[b] (CRM)CO_2/CH_4 = 1	289.3	307.4 (2.5)	0.15	7.4	0.8	0.11

[a] Contamination carbon was taken as reference at 284.6 eV. BE La $3d_{5/2}$ = 834.5 eV.
[b] Catalysts calcined and tested in reactions at 823 K.
[c] FWHM are given between parenthesis.
[d] Reduced in the pre-treatment chamber of the instrument.

Table 3
Binding energies[a] and surface concentration for $Rh(0.6)/La_2O_3(27)–SiO_2$.

Treatment at 823 K	Rh $3d_{5/2}$[c] (eV)	O 1s (eV)	Rh/La + Si	O/La + Si
Calcined[b]	308.8 (3.4)306.4 (3.1)	531.6	0.0027	–
H_2, in situ[d] at 723 K	306.8 (3.0)	531.9	0.0027	–
Used in CR (CRM)[b] $CO_2/CH_4 = 1$	307.6 (3.1)	531.9	0.0027	1.4
Used in CR (CRM)[b] $CO_2/CH_4 = 1.9$	307.6 (3.1)	532.0	0.0030	1.3
Used in MR (CRM)[b] $CO_2/CH_4 = 1.9$	307.4 (3.1)	531.9	0.0028	1.27
Used in MR (DRM)[b] $CO_2/CH_4 = 1$	307.6 (3.0)	531.9	0.0028	–

[a] Contamination carbon was taken as reference at 284.6 eV.
BE La $3d_{5/2}$ = 834.9 eV, Si 2s = 153.7 eV.
[b] Catalysts calcined and tested in reactions at 823 K.
[c] FWHM are given between parentheses.
[d] Reduced in the pre-treatment chamber of the instrument.

constant after the different treatments (Table 3), suggesting that no significant change in the rhodium dispersion occurred. The C 1s spectra only showed one well-defined peak at 284.6 eV. No peak at 289.1 ± 0.2 eV, attributed to carbonate carbon was observed.

4. Conclusions

Both catalysts are very active and stable when used in either conventional or membrane reactors for hydrogen production with or without oxygen in the feed. This behavior is consistent with the very low formation of graphitic deposits (only detected through LRS). In previous studies [3,4], it was shown that this stability was mainly due to the strong metal–support interaction operating in both systems.

Through an adequate reactor design, it was possible to avoid the exposure of the membrane to oxygen containing atmospheres, thus extending the durability of the membrane. As of this writing the reactor has been on CRM stream for 1800 h. In the upper part of the catalyst bed (Fig. 1), the reaction system reaches equilibrium. Thus, the role of the catalyst in contact with the membrane is to restore equilibrium as H_2 is extracted through the inner tube wall (Fig. 6).

The addition of O_2 to the reactant feed not only improves the energy balance but also increases both methane conversion and H_2 production and recovery. In all cases, the binary oxide supported Rh performs better than $Rh(0.6)/La_2O_3$. By increasing the CO_2/CH_4 feed ratio between 0.5 and 1.9 in the membrane reactor, both methane conversion and H_2 production are improved.

This study opens up an avenue of research concerning the application of membrane reactors to the production of hydrogen co-feeding oxygen with the reactants trying to reach the thermal balance between the exothermic and endothermic reactions.

Acknowledgments

The authors wish to acknowledge the financial support received from UNL, CONICET and ANPCyT. Thanks are also given to the Japan International Cooperation Agency (JICA) for the donation of the XRD, to ANPCyT for the purchase of the Raman instrument (PME 87-PAE 36985) and the UHV Multi Analysis System (PME 8 – 2003), and to Prof. Elsa Grimaldi for the English language editing.

References

[1] J.F. Múnera, S. Irusta, L.M. Cornaglia, E.A. Lombardo, D.V. Cesar, M. Schmal, Kinetic and reaction pathway of the CO_2 reforming of methane on Rh supported on lanthanum-based solid, J. Catal. 245 (2006) 25–34.
[2] J.F. Múnera, L.M. Cornaglia, D.V. Cesar, M. Schmal, E.A. Lombardo, Kinetic studies of the dry reforming of methane over the $Rh/La_2O_3–SiO_2$ catalyst, Ind. Chem. Eng. Res. 46 (23) (2007) 7543–7549.
[3] S. Irusta, J. Múnera, C. Carrara, L.M. Cornaglia, E.A. Lombardo, A stable novel catalyst improves hydrogen production in a membrane reactor, Appl. Catal. 287 (2) (2005) 147–158.
[4] L.M. Cornaglia, J. Múnera, S. Irusta, E.A. Lombardo, Raman studies of Rh and Pt on La_2O_3 catalysts used in a membrane reactor for hydrogen production, Appl. Catal. 263 (1) (2004) 91–101.
[5] F. Gallucci, S. Tosti, A. Basile, Pd–Ag tubular membrane reactors for methane dry reforming: a reactive method for CO_2 consumption and H_2 production, J. Membr. Sci. 317 (2008) 96–105.
[6] P. Ferreira-Aparicio, M. Benito, K. Kouachi, S. Menad, Catalysis in membrane reformers: a high-performance catalytic system for hydrogen production from methane, J. Catal. 231 (2005) 331–343.
[7] N. Aishah, S. Amin, T. Chun, T.C. Yaw, Thermodynamic equilibrium analysis of combined carbon dioxide reforming with partial oxidation of methane to syngas, Int. J. Hydrogen Energy 32 (2007) 1789–1798.
[8] A. Donazzi, A. Beretta, G. Groppi, P. Forzatti, Catalytic partial oxidation of methane over a 4% Rh/α-Al_2O_3 catalyst Part II: role of CO_2 reforming, J. Catal. 255 (2008) 259–268.
[9] M. Simeone, L. Salemme, D. Scognamiglio, C. Allouis, G. Volpicelli, Reactor temperature profile during autothermal methane reforming on Rh/Al_2O_3 catalyst by IR imaging, Int. J. Hydrogen Energy 33 (18) (2008) 4798–4808.
[10] F. Roa, J.D. Way, The effect of air exposure on palladium–copper composite membranes, Appl. Surf. Sci. 240 (1–4) (2005) 85–104.
[11] C. Huang, A. T-Raissi, Thermodynamic analyses of hydrogen production from sub-quality natural gas. Part II: steam reforming and autothermal steam reforming, J. Power Sources 163 (2007) 637–644.
[12] M.M.V.V. Souza, M. Schmal, Combination of carbon dioxide reforming and partial oxidation of methane over supported platinum catalysts, Appl. Catal. A 225 (2003) 83–92.
[13] W. Wang, S.M. Stagg-Williams, F.B. Noronha, L.V. Mattos, F.B. Passos, Partial oxidation and combined reforming of methane on of methane on Ce-promoted catalysts, Catal. Today 98 (2004) 553–563.
[14] C. Carrara, A. Roa, L. Cornaglia, E.A. Lombardo, C. Mateos-Pedrero, P. Ruiz, Hydrogen production in membrane reactors using Rh catalysts, Catal. Today 133 (2008) 344–350.
[15] H. Vidal, S. Bernal, R.T. Baker, G.A. Cifredo, D. Finol, J.M. Rodríguez-Izquierdo, Catalytic behavior of lanthana promoted Rh/SiO_2 catalysts: influence of the preparation procedure, Appl. Catal. A 208 (2001) 111–123.
[16] C. Klinke, R. Kurt, J.M. Bonard, K. Kern, Raman spectroscopy and field emission measurements on catalytically grown carbon nanotubes, J. Phys. Chem. B 106 (43) (2002) 11191–11195.
[17] A.M. Connor, J.R. Ross, The effect of O_2 addition on the carbon dioxide reforming of methane over Pt/ZrO_2 catalysts, Catal. Today 46 (1998) 203–210.
[18] V.I. Nefedov, M.N. Firsov, I.S. Shaplygin, Electronic structures of $MRhO_2$, $MRh2O_4$, $RhMO_4$ and Rh_2MO_6 on the basis of X-ray spectroscopy and ESCA data, J. Electron Spectrosc. Relat. Phenom. 26 (1982) 65–78.
[19] H.J. Gysling, J.R. Monnier, G. Apai, Synthesis, characterization, and catalytic activity of $LaRhO_3$, J. Catal. 103 (1987) 407.
[20] K. Polychronopoulou, J.L. Fierro, A.M. Efstathiou, The phenol steam reforming reaction over MgO-based supported Rh catalysts, J. Catal. 228 (2004) 417–432.
[21] G.R. Gallaher, J.G. Goodwin, Ch.Sh. Huang, M. Houalla, XPS and reaction investigation of alkali promotion of Rh/La_2O_3, J. Catal. 140 (1993) 453–463.
[22] S. Lacombe, C. Geantet, C. Mirodatos, Oxidative coupling of methane over lanthana catalysts. I. Identification and role of specific active sites, J. Catal. 151 (1994) 439–452.
[23] S. Zafeiratos, V. Nehasil, S. Ladas, X-ray photoelectron spectroscopy study of rhodium particle growth on different alumina surfaces, Surf. Sci. 433 (1999) 612–616.
[24] S. Labich, E. Taglauer, H. Knozinger, Metal–support interactions on rhodium model catalysts, Top. Catal. 14 (2001) 153–161.